International Journal of Civil Engineering

Geotechnical Engineering

Use of centrifuge experiments and discrete element analysis To model the reverse fault slip

Y.Y. Chang[1], C.J. Lee[1,*], W.C. Huang[1], W.J. Huang[2], M.L. Lin[3], W.Y. Hung[4], Y. H. Lin[5]

Received: February 2013, Accepted: May 2013

Abstract

This study presents a series of physical model tests and numerical simulations using PFC^{2D} (both with a dip slip angle= 60° and a soil bed thickness of 0.2 m in model scale)at the acceleration conditions of 1g, 40g, and 80 g to model reverse faulting. The soil deposits in prototype scale have thicknesses of 0.2 m, 8 m, and 16 m, respectively. This study also investigates the evolution of a surface deformation profile and the propagation of subsurface rupture traces through overlying sand. This study proposes a methodology for calibrating the micromechanical material parameters used in the numerical simulation based on the measured surface settlements of the tested sand bed in the self-weight consolidation stage. The test results show that steeper surface slope on the surface deformation profile, a wider shear band on the major faulting-induced distortion zone, and more faulting appeared in the shallower depths in the 1-g reverse faulting model test than in the tests involving higher-g levels. The surface deformation profile measured from the higher-g physical modeling and that calculated from numerical modeling show good agreement. The width of the shear band obtained from the numerical simulation was slightly wider than that from the physical modeling at the same g-levels and the position of the shear band moved an offset of 15 mm in model scale to the footwall compared with the results of physical modeling.

Keywords: *Reverse fault, Surface deformation profile, Subsurface rupture trace, Centrifuge modeling, Discrete element method*

1.Introduction

Permanent ground deformation caused by normal and reverse fault rupture has caused serious damage to man-made structures overlying on a fault trace in recent large earthquakes. During three destructive earthquakes, Turkey (Kocaeli and Düzce)[1] and Taiwan(Chi-Chi)in 1999, several man-made structures were destroyed because of foundation displacements caused by fault rupture propagation from the base rock to the ground surface [2]. Therefore, the determination of setback distances is necessary to avoid earthquake-induced damages. Evidence from the 1999 Taiwan Chi-Chi Earthquake shows that regulations in the Taiwan Seismic Code for urban dense population areas regarding the setback distances from a surface rupture must be revised. Minimum setback distances are required if structures are adjacent to an active fault line. Hence, the guidance for evaluating a potential surface rupture zone and the issues related to the extent of ground surface deformation are becoming important. Researchers typically apply following three approaches to study these issues: (1) field studies of case history [3, 4]; (2) 1 g (g=9.8 m/s^2) and geotechnical centrifuge experiments [5, 6]; and (3) numerical modeling such as finite element methods [7, 8, 9] and finite difference methods [10, 11]. Recent studies have provided a better understanding of the effects of faulting on ground surface deformation. The usage of the finite element method to model the propagation of a fault rupture through soils is the most common numerical method. The discrete element method (DEM) has recently become popular due to capturing the behavior of particulate materials. Researchers have used the DEM to solve real problems that involve complex deformation patterns because it has the advantage of solving large deformation problems such as fault ruptures. However, this approach has not been used to evaluate the fault rupture propagation problem.

This study investigates the evolution of surface deformation profiles and the propagation of subsurface rupture traces

* *Corresponding Author: cjleeciv@ncu.edu.tw*
1 Department of Civil Engineering. National Central University, Taiwan.
2 Department of Applied Geology Engineering. National Central University, Taiwan.
3 Department of Civil Engineering. National Taiwan University, Taiwan.
4 National Center for Research on Earthquake Engineering, Taiwan.
5 Central Geological Survey, MOEA, Taiwan

induced by reverse faulting through overlying sand by using both centrifuge experiments and the numerical simulation of PFC^{2D} (Particle Flow Code)[12]. The centrifuge experiments in this study initiated the reverse faulting of a dip angle of 60^{o} (at the bedrock level) through the overburden sand layer and emerging on the ground surface. The measured surface deformation profiles at various throws provided the validation of numerical experiments. This study also presents a numerical methodology and a method for calibrating the micromechanical material parameters used in PFC^{2D} simulation to analyze the reverse fault propagation through the overburden sand layer.

2. Geotechnical Centrifuge modeling

2.1 Testing equipment

The experiments in this study were undertaken in the beam centrifuge at National Central University (NCU), Taiwan. The NCU Geotechnical Centrifuge has a nominal radius of 3 m and integrates a 1D servo-hydraulically controlled shaker with a swing basket. The dimensions of the NCU centrifuge platform are 100 cm×55 cm×72 cm (length × width ×height), and the maximum payload of the platform is 400 kg at an acceleration of 80 g(32 g-ton)[13].

The fault simulation container, shown in Fig. 1, was designed to conform to the dimensions and load capacity of the NCU centrifuge platform. The dimensions of the fault simulation container are 100 cm×52.8 cm×67.5 cm (length×width×height). The container can simulate the normal/reverse fault slip with the speed of 0-2.5 mm/min in displacement control mode. The maximum vertical throw (uplift and falling height) can reach 5.5 cm. A space of 74cm in length, 30cm in width, and 32.5cm in height was provided for the tested soil bed in the container. An L-shape push panel with the dimensions of 15cm × 30cm × 25 cm was manufactured to push the tested soil bed upward (reverse faulting) or pull the tested soil bed downward (normal faulting) with a dip angle of 60°. An acrylic window of 60 cm×28.15 cm was used to observe the subsurface deformation profiles during faulting. The container and the related devices were tested at a maximum acceleration of 80 g. The normal and reverse faulting tests were performed using the fault simulation container.

An in-flight surface profile scanner (Fig. 2) equipped with two laser displacement transducers installed horizontally and vertically and driven with a motor could densely scan the surface elevation on the center line of the tested sand bed during both normal and reverse faulting tests. Figure 3 shows the simplified geometry of the overburden soil layer and the fault tip of reverse fault to be modeled in the centrifuge. Figure 4 shows the dimensions of the fault simulation container and the coordinate system used to demonstrate the testing results in the following sections. As shown in Figs. 3 and 4, the origin of the coordinate system is the point at which the fault tip projects to the surface.

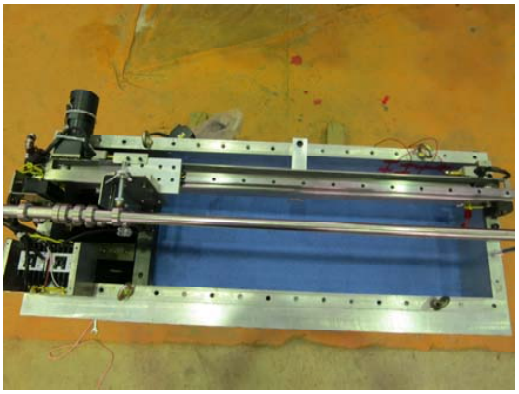

Fig. 2 In-flight surface profile scanner

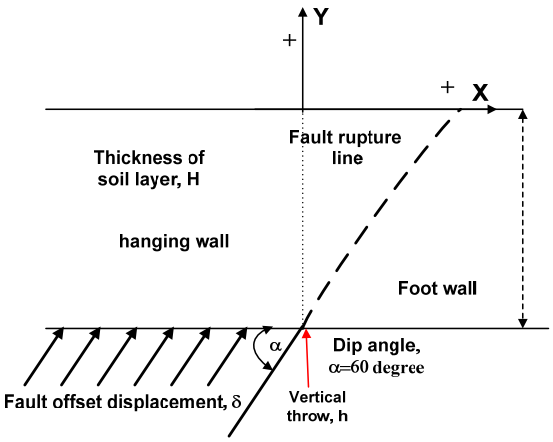

Fig. 3 Geometry of overburden soil layer and the fault tip of the reverse fault

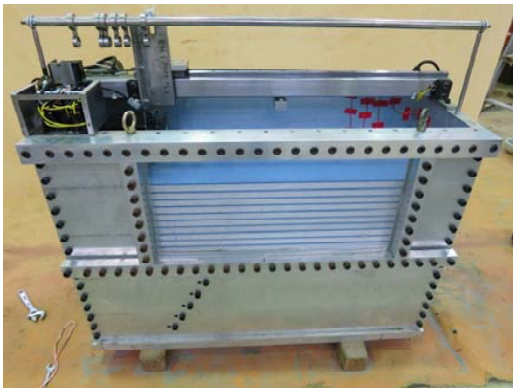

Fig. 1 Fault simulation container

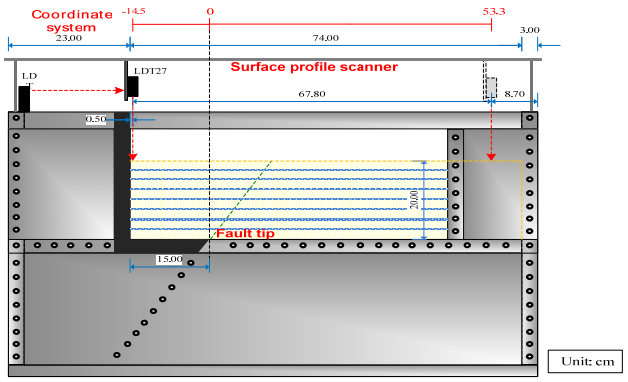

Fig. 4 Dimensions of the fault simulation container and the coordinate system used in the study

2.2 Tested Sand, Sand Bed Preparation, Testing Setup, and Testing Conditions

Crushed quartz sand was used to prepare the uniform sand bed for all the tests in this study. Fine uniform silica sand has the D_{50}=0.149 mm, ρ_{max}=1660kg/m^3, ρ_{min}=1380 kg/m^3. A peak friction angle ϕ_{peak}=41^o, and a dilation angle φ=6^o was measured with the direct shear tests for the sand with a relative density of 70% at a normal stress=200kPa. The dry quartz sand was pluviated from a hopper with a regular path into the container at a specified falling height and a constant flow rate to prepare fairly uniform sand deposits with a relative density of approximately 70%. Figure 5 shows the sand pluviator on the fault simulation container for preparing the tested sand bed. The pluviation process was interrupted as needed to spray a thin layer of blue dyed sand at specified elevations as marker layers in proximity to the acrylic window to allow identification of shear deformation in the subsurface. A sand bed 20 cm thick was prepared to correspond to 16 m on the prototype scale when tested at an acceleration of 80 g. The soil bed had prototype scale dimensions of 59.2m×24m×16m and a maximum vertical throw of 4 m. After completing the centrifuge flight safety checks, the centrifuge was accelerated at an acceleration of 10 g per step until it reached the target accelerations (40 g and 80 g). In each step, the surface profile scanner was trigged to scan the surface profile to measure the surface settlement caused by increased g levels. Once the centrifuge reached the target acceleration, reverse faulting was conducted. The fault throw increased at a constant velocity of 2 mm/min using an AC motor. The surface profile scanner was driven once to scan the surface elevations per 2.5 mm-throw increment. The fault displacement increased until reached a final throw of 5 cm (corresponding to 4 m at the prototype scale). Table 1 shows the testing program. This study presents three reverse faulting tests performed at three different g levels (1 g, 40 g, and 80 g). Here the notation of "#g"in the test number represents the test performed at #g, and "Rtest#" represents the serial number of the reverse faulting test.

Fig. 5 Sand pluviator on the fault simulation container

2.3 Testing results and interpretations of physical modeling

The tested sand bed 20 cm thick was confined to the container, and no lateral deformation was allowed. Therefore, the sand beds tested at each glevel would experience self-weight consolidation in the at-rest (k_0) state. Figure 6 displays the relationship between the measured surface settlements (in model scale) and the effective overburden stresses at a depth of 10 cm (in model scale)at various g levels. The constrained modulus, $M_{physical}$, for the tested soil bed is

$$\mathrm{M}_{physical} = \frac{\sigma_v'}{\varepsilon_v} = \frac{(1-v)}{(1+v)(1-2v)} E \qquad (1)$$

Where σ_v'=effective overburden stress, ε_v= vertical strain, E=Young's modulus, and v=Poisson's ratio. Therefore, the average constrained modulus of the sand bed at various stress levels obtained from physical modeling, $M_{physical}$, can be calculated using Eq.1. The value of $M_{physical}$, depends on the effective overburden stress, and the empirical relationship between the average constrained modulus and the stress levels can be formulated as follows:

$$M_{physical}=B(\sigma_v')^m \qquad (kPa) \qquad (2)$$

Where B=4631 and m=0.4 produce the best curve fitting results for the tested sand bed (Fig. 7).

At the target accelerations(1 g, 40 g, and 80 g), the reverse faulting was actuated by the L-shape panel moving upward along the dip angle of 60^o. The progressive rupture failure was observed as the vertical throw, h, (assuming positive value in the reverse faulting tests) increased. The vertical throw, h, was obtained from the uplift height of the L-shape panel. The surface deformation profiles measured at various vertical throws can be plotted based on the previously defined coordinate system. The ratio of the vertical throw to the thickness of the overburden soil, r (%), is defined as

$$r(\%)=h/H\times 100 \qquad (3)$$

Table 1 Reverse fault testing program

Test No.	Height of specimen (mm)	Relative density (%)	tested g-level (g)	Max. throws of Fault (mm)
1gRtest20	200	70	1	50
40gRtest21	200	70	40	50
80gRtest23	200	70	80	50

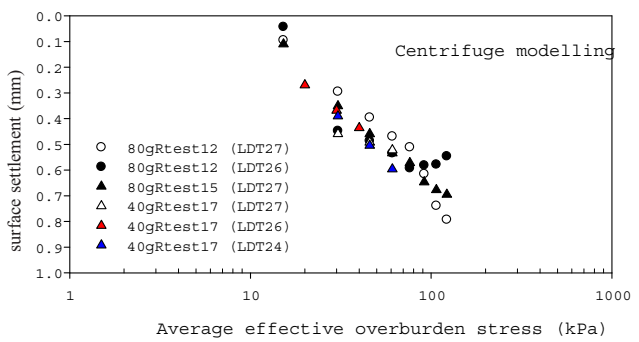

Fig. 6 Relation of the measured surface settlement and average effective overburden stress

The maximum vertical throw was +5 cm (r=25%) in the tests. The surface deformation profile was measured per vertical throw of 2.5 mm. Each test included 20 measured surface deformation profiles (S1 – S20).

Figure 8(a) shows the surface deformation profiles at various r values ranging from 1.25% to 25% for the reverse faulting test of 80gRtest23. Figure 8(b) shows the relative positions of the surface deformation profiles and the fault tip. As expected, the uplifting height increases with the vertical throw. The surface deformation profile and the maximum uplift height start at the position of approximately -60 mm from the fault tip. Figure 9 shows a comparison of the measured surface deformation profiles tested at 1 g, 40 g, and 80 g. The surface deformation profiles obtained from 1 g tests have the steeper surface slopes than those appearing in the tests for higher g levels.

Figure 10 shows photos of the subsurface deformation profiles taken from the acrylic window after the reverse faulting tests (h = 5 cm) at accelerations of 1 g, 40g, and 80g,

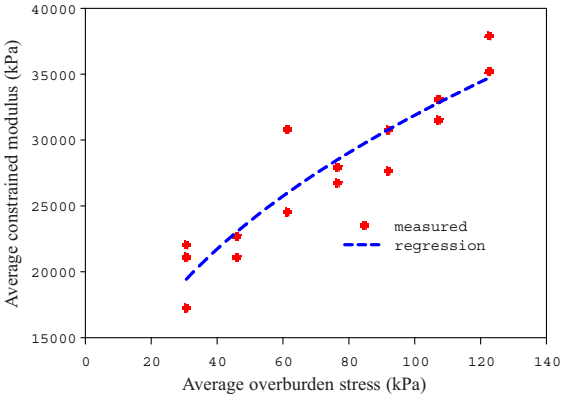

Fig. 7 Relation of the measured constrained modulus and the average effective overburden stress

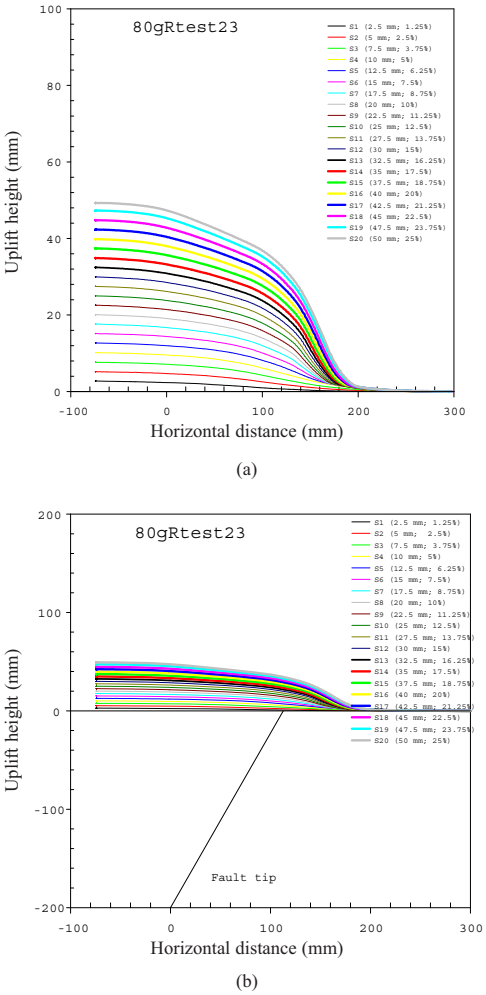

Fig. 8 Surface deformation profiles at various throws for reverse faulting (80gRtest23): (a) detailed surface deformation profiles; (b) the relative positions of the surface deformation profiles and the fault tip (Both dimensions in model scale)

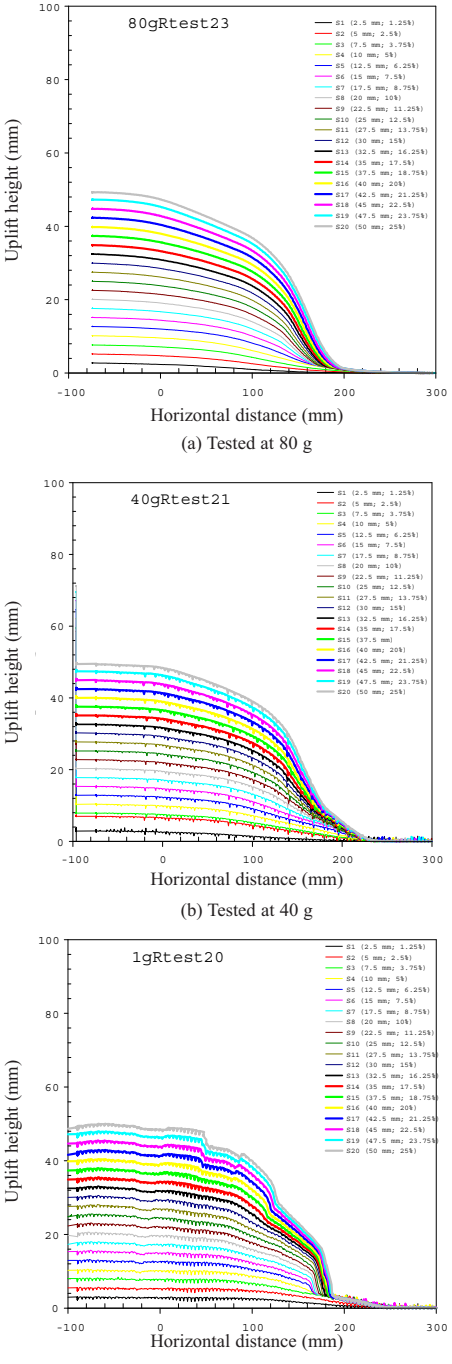

Fig. 9 Comparison of surface deformation profiles tested at different g-levels on reverse faulting: (a) 80 g; (b) 40 g; (c) 1 g

respectively. The 10 thin-colored sand marker layers in the soil bed provide a better visual picture of the rupture pattern after testing. A digitizer software were used to trace and mark the deformation shape of each soil layer as shown in Fig. 11. By connecting the rupture paths of each soil layer, two major rupture paths can be plotted and a distortion zone between two major paths can be defined. Digitizer software was then used to convert the selected points on the image of the subsurface deformation profile into digital representations (Fig. 11). The fault rupture lines and their relative positions can then be converted into digital format for digital processing and management. Figure 12 (a) shows that the upper bound (black

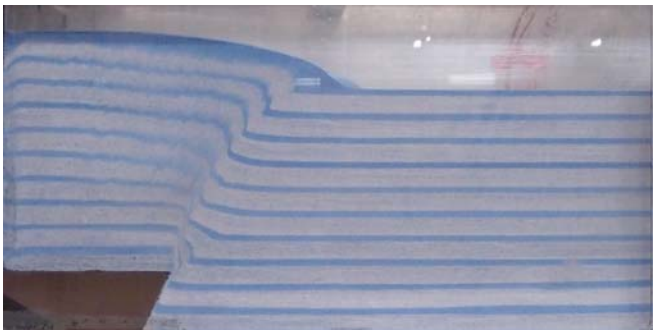

(a) tested at 80 g

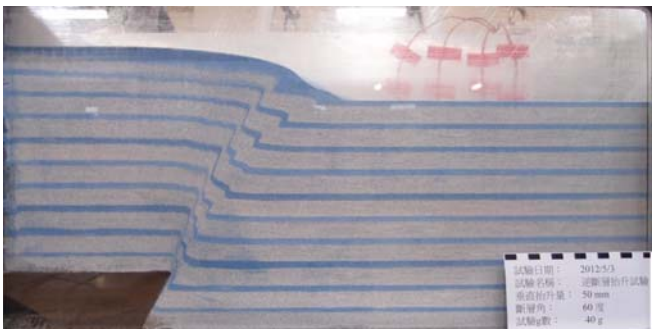

(b) tested at 40 g

(c) tested at 1 g

Fig. 10 Photos of subsurface deformation patterns tested at different g-levels after 5-cm-throw reverse faulting: (a) 80 g; (b) 40 g; (c) 1 g

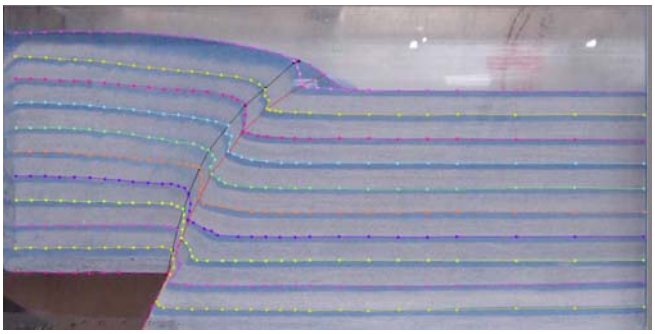

Fig. 11 Digitization on the image of subsurface deformation profile for 80gRtest23

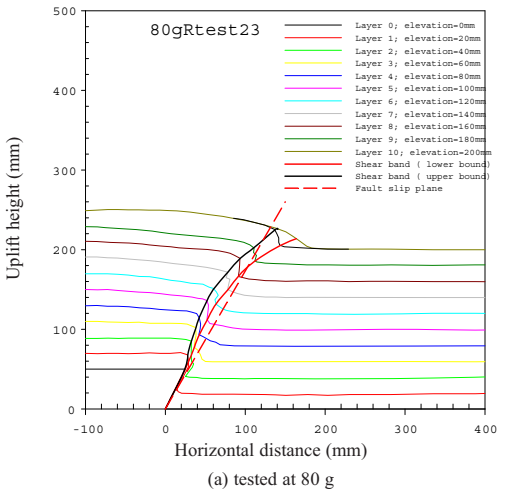

(a) tested at 80 g

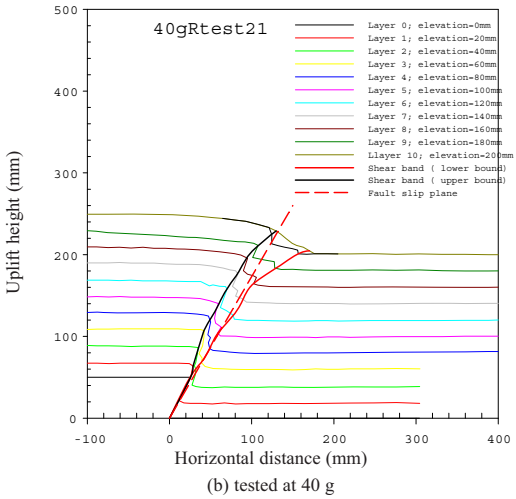

(b) tested at 40 g

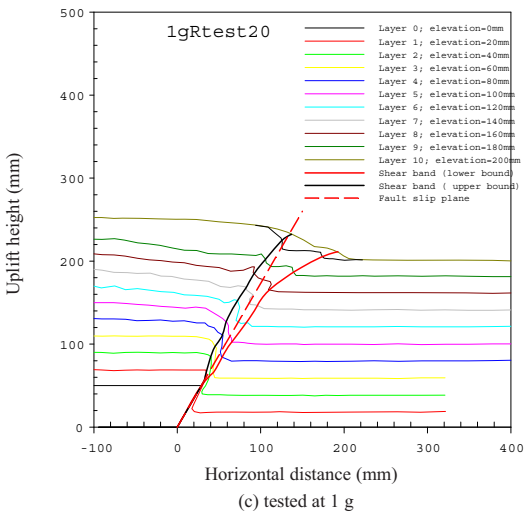

(c) tested at 1 g

Fig. 12 Comparison of major shear-induced distortion zone tested at different g-levels for reverse faulting: (a) tested at 80 g; (b) tested at 40 g; (c) tested at 1 g

line) and the lower bound (red line) of the rupture path obtained by connecting the points with minimum radiuses of curvature on each marker layer for 80gRtest23. These rupture paths initially extended along the dip plane, but curved out over the footwall. The zone confined within the upper bound and the lower bound is the major faulting-induced distortion zone. Figures 12 (b) and 12(c) show the major faulting-induced distortion zone for 40gRtest21 and 1gRtest20, respectively. The major distortion zone is defined as the shear band caused by reverse faulting. The underground structures embedded within the shear band would undoubtedly suffer serious damage.

After examining the subsurface deformation patterns in the shallower depths as shown in Figs 10(a)-10(b), we found that more faulting lines were developed in the 1-g reverse faulting test than in the higher g reverse faulting tests. The major faulting-induced distortion zones appeared in the sand beds, when tested at 1 g, 40 g, and 80 g, differ significantly(Figs. 12(a) to 12(c)). The distorted zone induced by the reverse faulting tested at 80 g has the narrowest width of shear band, whereas that induced by the reverse faulting tested at 1 g has the widest shear band width. The distorted zone induced by the reverse faulting tested at 40 g lies in between. These results might be caused by following two possible mechanisms: (I) the small capillarity force developed between the sand particles(apparent cohesion), which increases the effective stresses in the soil mass. (II)the higher rate of dilation occurred when the soil mass was sheared in the lower confined stress (tested at the lower g level or in the shallower depth of sand bed) [14]. Centrifuge reverse faulting tests can precisely simulate in-situ stress levels, and are absolutely necessary for investigating the field reverse fault mechanism.

3. Discrete element method

3.1. Numerical simulation of PFC^{2D}

Previous researchers have used the DEM to examine the macro/micro mechanical behaviors of granular materials based on the results of experimental testing [15, 16]. PFC^{2D} is a 2D discrete element computer code for simulating the mechanical behavior of granular assemblies[12]. This study uses the PFC^{2D} to analyze the phenomenon of reverse fault rupture propagation from the base rock through the overlying sand to the ground surface. The simulations in this study take advantage of a linear contact model and a slip model defined by the normal and shear stiffness K_n and K_s and the friction coefficient at the contact, μ, for the two contact entities (ball-to-ball and ball-to-wall).

3.2. Generation of numerical specimen for PFC^{2D} analysis

The domain of numerical simulation in this study is defined with five rigid walls (Wall 1, Wall 2, Wall 3, Wall 4, and Wall 5) as shown in Fig. 13. The distance from Wall 3 to Wall 4 is 1000 mm, which is longer than the length of the tested sand bed (740 mm; Fig. 4). The use of a longer specimen in the numerical analysis enables a similar numerical simulation on the fault rupture events with smaller dip angles (<60°), and avoids the possible boundary effects from the wall. Wall 2 and Wall 3 are fixed walls, and Wall 1, Wall 4, and Wall 5 are moving walls with amoving vector of 60° along the predetermined fault rupture plane.

Figure 14 shows the grain size distribution of the tested sand used in the centrifuge experiments, where the mean grain size, D_{50}, is 0.149 mm. The specimen used in the numerical simulation of PFC^{2D} consisted of 28 759 with three radii: 1.49 mm, 1.05 mm, and 0.74 mm. The size distribution curve of the circular disk is parallel to the grain size distribution curve of the tested sand (i.e., real sand; Fig.13). The mean grain size, D_{50}, of circular disks is 2.98 mm, which is approximately 20 times larger than that of the tested sand. The numerical specimen was constructed by randomly pluviating the mixed disks into the box confined with the 4 walls, layer by layer. Each 20-mm-thick layer consisted of 1578 mixed disks, and 50 thin layers were initially stacked. The stacked layers were then subjected to 1-g self-weight consolidation until the average unbalance-force ratio was less than 0.01. Removing the disks located over the elevation of 200 mm formed the final numerical specimen of 200 mm in thickness, which is the same as the tested sand bed. Figure 14 shows the dimensions of the numerical specimen and the coordinate system used to demonstrate the numerical results in the following sections. The coordinates of the fault tip used in the PFC^{2D} simulation modeling and in the centrifuge modeling are the same. The disks at elevations of approximately 2, 4, 6, 8, 10, 12, 14, 16, 18, and 20 mm were marked with red as the marker layers, as shown in Fig. 14, and can be continuously traced to their positions during the simulation of the reverse faulting event. This prepared specimen was used in the following numerical analysis.

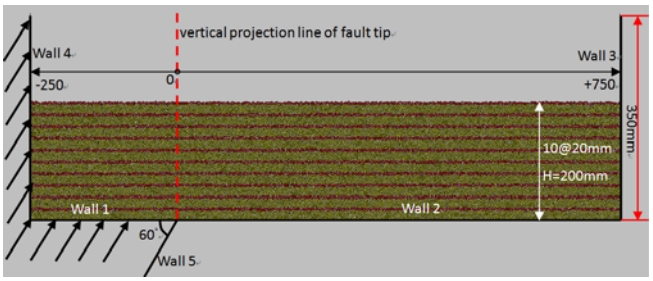

Fig. 13 Problem geometry, imposed reverse faulting boundary conditions and dimensions of PFC^{2D} numerical simulation

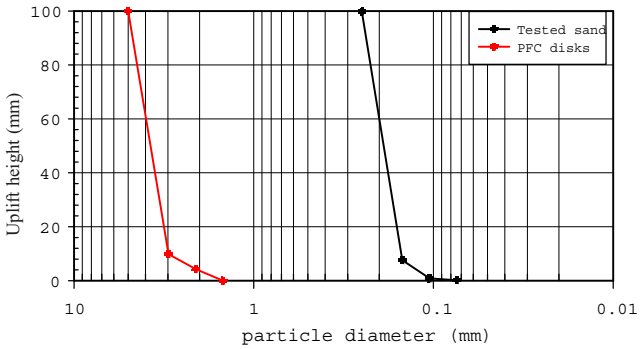

Fig. 14 Grain size distribution curves of PFC^{2D} modeling and the test sand

3.3. Calibration of the parameters for PFC^{2D} analysis

The input material parameters used in PFC^{2D} analysis include the normal and shear stiffness of the disks, K_n and K_s , the normal and shear stiffness of walls, K_{nw} and K_{sw}, the density of disks, ρ, and the friction coefficient, μ, between the disks and between the disk and the wall. These micro-material parameters must be calibrated before performing the numerical simulation. This study proposes a calibration methodology and procedure based on a comparison of the surface settlements of the tested sand bed measured from 1 to 80 g and the surface settlements of numerical specimens calculated in the self-weight consolidation stage using numerical simulations.

The effective overburden stress at a depth of D for any g level in the numerical specimen can be calculated using Eq. 4, as in physical modeling:

$$\sigma_v'=\rho NgD \tag{4}$$

where ρ=density of the disk, and Ng= N times the earth gravity if the Ng situation is simulated in the numerical modeling. Hence, we can numerically model the behavior of the soil deposit with various thicknesses in the prototype by subjecting various glevels to the same numerical specimen (Fig. 14). The unit weight of the tested sand bed at 1g (the earth gravity) is 15.35kN/m^3. The density of the disk, ρ, was set at 1850 kg/m^3 so that the effective overburden stress at the corresponding depths between the physical model and the numerical specimen have the same values at any tested (physical model) or simulated (numerical model) glevel (1 to 80 g).

Yimsiriand Soga [17] proposed a micro mechanical-based stress-strain model based on micromechanics theory for anisotropic and isotropic granular material at small strains. They proposed the following relationships between macroscopic parameters E and v (Young's modulusand Poisson's ratio, respectively) and microscopic material parameters (K_n, K_s, r, N, and V) for an isotropic granular assembly:

$$\mathrm{E}=\frac{4\mathrm{r}^2\mathrm{N}}{9\mathrm{V}}\left[\frac{15\mathrm{K_n}\mathrm{K_s}}{2\mathrm{K_n}+3\mathrm{K_s}}\right]=\frac{4r^2N}{9V}\left[\frac{15K_n}{2\frac{K_n}{K_s}+3}\right] \tag{5}$$

$$\mathrm{G}=\frac{4\mathrm{r}^2\mathrm{N}}{9\mathrm{V}}\left[\frac{15\mathrm{K_n}\mathrm{K_s}}{6\mathrm{K_n}+4\mathrm{K_s}}\right]=\frac{4r^2N}{9V}\left[\frac{15K_n}{6\frac{K_n}{K_s}+4}\right] \tag{6}$$

$$v=\frac{5(K_n-K_s)}{10K_n+3K_s}=\frac{\frac{K_n}{K_s}-1}{2\frac{K_n}{K_s}+3} \tag{7}$$

where r = radius of the particle, N = coordinate numbers of the particle, and V=volume of assembly.

Equation 7 shows that v depends on the ratio of normal stiffness and shear stiffness, K_n/K_s . The settlement behavior of the sand bed confined in the fault simulation container in the self-weight consolidation stage (increases of g level) is stressed in the at-rest condition (K_o condition). The coefficient of earth pressure at rest is approximately related to the effective friction angle by the following formula:

$$K_o\approx(0.95-\sin\phi') \tag{8}$$

The sand in the stress state of the at-rest condition does not involve failure of sand and may represent a state of elastic equilibrium. Therefore, the coefficient of earth pressure at rest can be represented with Poisson's ratio, and is written as

$$K_o=\frac{v}{1-v} \tag{9-a}$$

and $$v=\frac{K_o}{1+K_o} \tag{9-b}$$

The effective internal friction angle of the tested sand, (ϕ_{peak}), is equal to 41°, leading to K_o=0.294 (Eq. 8) and v=0.227 (Eq. 9-b). Substituting v=0.227 into Eq. 7, the ratio of the normal stiffness to the shear stiffness (K_n/K_s) is equal to 3.07, and we consequently assume that K_n/K_s =3 in the study.

The disks are used to simulate the sand grains in a stress state of the at-rest condition in the PFC^{2D} simulation. Therefore, the constrained modulus, $M_{numerical}$, in terms of E and v, is written as

$$\mathrm{M}_{numerical}=\frac{\sigma_v}{\varepsilon_v}=\frac{E}{1-v^2} \tag{10}$$

Assuming that K_n/K_s =3 and then substituting E(Eq.5) and v (Eq.7) into Eq.10, $M_{numerical}$ in terms of the microscopic parameters can be written as

$$M_{numerical}=f(e)AK_n \tag{11}$$

where $f(e)$ is a function of the void ratio, and A is a constant related to the ratio of the normal stiffness and the shear stiffness. Therefore, the value of $M_{numerical}$ depends only on the normal stiffness. Similarly, assuming that K_n/K_s=3 and substituting E (Eq.4) and v (Eq.6) into Eq.1, the constrained modulus of the centrifuge physical model, $M_{physical}$, can be written in the following microscopic parameters:

$$M_{physical}=f(e)BK_n \tag{12}$$

The settlement behavior of the sand bed confined to the fault simulation container in the self-weight consolidation (increasing g level to the target acceleration) is stressed in the at-rest condition (K_o condition). Hence, the measured $M_{physical}$ can be used to calibrate the value of K_n used in the PFC^{2D} analysis.

Equation 2 shows that the constrained modulus increases with the effective overburden stress for the centrifuge models. Therefore, we assume that the normal stiffness increases as the effective overburden stress, σ_v', increases for the numerical specimen. The relationship of K_n and σ_v' can be expressed as

$$\mathrm{K}_n=K_{no}\left(\frac{\sigma_v'}{\sigma_{vo}'}\right)^{0.4} \tag{13}$$

where σ_{vo}'= the effective overburden stress at the depth of 1 cm, and K_{no}= the normal stiffness at σ_{vo}'. The peak friction angle of the granular material can be represented as the sum of the sliding resistance at contacts, particle rearrangements, and dilation. This study uses the numerical specimen to simulate the shear behavior of the sand deposit(Dr=70%) with a ϕ_{peak}=41^o, a dilation angle of φ=6^o, and a friction coefficient between disks equal to 0.73 (ϕ=36^o).

After determination of the ratio of normal and shear stiffness (K_n/K_s=3), the friction coefficient (μ=0.73), and m=0.4 used in

Eq. 13 as a series of preliminary PFC^{2D} simulation using various normal stiffnesses (0.4×10^7, 0.5×10^7, 0.6×10^7 and 0.7×10^7 N/m) was iteratively performed for the calibration of the value of K_{no}. The numerical specimens were first subjected to the self-weight consolidation at the different g levels (from 1 to 80 g in 10g increments). The surface settlements at different g levels were then calculated. Figure 15 shows a comparison of the calculated settlements for various normal stiffness values and the measured settlements from the physical model at various g levels. Figure 16 shows a comparison of the calculated settlements of K_{no}=0.5×10^7 N/m and various m (m=0.3, 0.4, 0.45, and 0.5) and the measured settlements from the physical model at various g levels. Applying K_{no}=0.5×10^7 N/m and m=0.4 in the PFC^{2D} simulation produces results that are consistent with the measured settlements from centrifuge modeling. Hence, the numerical specimen and the parameters listed in Table 2 are capable of simulating the self-weight consolidation of the tested sand. After use of the calibrated parameters, the numerical reverse faulting was conducted for the moving Wall 1, Wall 4, and Wall 5 uplifting along the direction of the fault plane angle (60^o) at the conditions of 1 g, 40 g, and 80 g. The

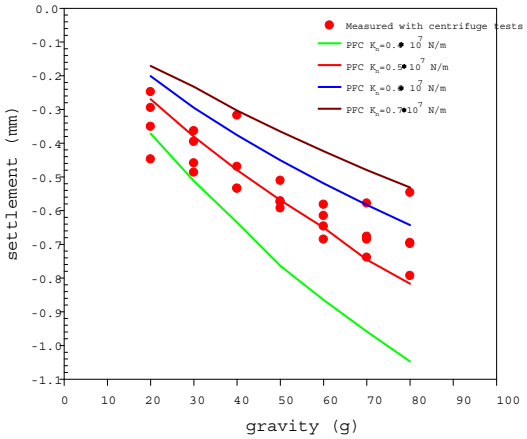

Fig. 15 Comparison between the calculated settlements derived by various normal stiffness and measured settlements from physical modeling at different g-levels

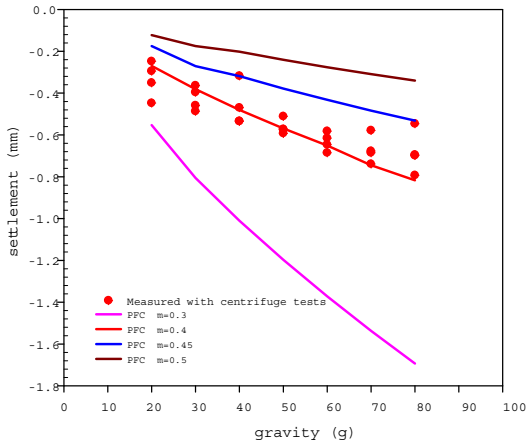

Fig. 16 Comparison of the calculated settlements of K_{no}=0.5×10^7 N/m and various m (m=0.3, 0.4, 0.45, and 0.5) and the measured settlements from the physical modeling at various g-levels

Table 2 Input parameters used in the study

Parameters	Values
Normal stiffness, K_n (N/m)	$K_n = K_{no}(\frac{\sigma_n'}{\sigma_{vo}'})^{0.4}$; K_{no}=0.5×10^7 N/m
Shear stiffness, K_s (N/m)	$1/3K_n$
Normal stiffness of walls	6.0×10^{12} N/m
Shear stiffness of walls	6.0×10^{12} N/m
Friction coefficient of between disks	0.73 ($\varphi = 36^o$)
Friction coefficient of between disks and wall	0.0
Density of disks (kg/m^3)	1850
Local damping coefficient	0.7 (default)

walls moved at a specified velocity of 2mm/min. The surface deformation profiles were then monitored at vertical throws of 1 cm, 2 cm, 3 cm, 4 cm, and 5 cm.

4. Experimental Results versus Numerical Simulation Results

The surface extent of the fault zone and subsurface rupture path propagation are two critical issues in measuring earthquake-induced damage. This study compares numerical results with the physical model test to determine surface deformation profiles at various throws. This study also compares the subsurface fault path images taken after the centrifuge tests with those derived from the PFC numerical simulationat the same vertical throws. Cross-verification of the numerical results and centrifuge experiment results provides a better understanding of the reverse faulting mechanism.

4.1 Comparisons of surface deformation profiles derived from numerical simulations and physical modeling

Figures17(a) - 17(c) show the surface deformation profiles measured from the physical model tests (represented with solid lines) and those obtained from the numerical simulations (represented with symbols) at vertical throws of 1 cm, 2 cm, 3 cm, 4 cm, and 5 cm and at conditions of 1 g, 40 g, and 80 g, respectively. Figure 17(a) shows the difference in the surface deformation profiles between the physical modeling and the numerical modeling at 1 g. This inconsistency may be attributed to the small capillary forces developing among the sand particles, which increase the effective stresses in the physical model but are not considered in the numerical simulation. In contrast, Figs. 17(b) and 17(c) show excellent agreement between the surface deformation profiles of the PFC^{2D} simulation and physical model. Thus, PFC^{2D} associated with the proposed calibration methodology of material parameters can reasonably predict the surface deformation profiles at various vertical throws during reverse faulting events.

4.2 Comparisons of subsurface rupture path propagation obtained from the numerical simulation and from the images taken from the physical model tests

Figure 18 shows the final rupture pattern of the marked layers after being subjected to a 5 cm throw in a numerical specimen simulated at 80 g. This detailed rupture pattern is

similar to the results obtained from the centrifuge model test in Fig. 10 and the field investigation involving the trenching of a fault scarp. This is the major benefit of using the DEM to model the fault slip. The symbols shown in Figs. 19(a) – 19(c) represent the final elevations of the marked layer at various elevations. The major faulting-induced distortion zone

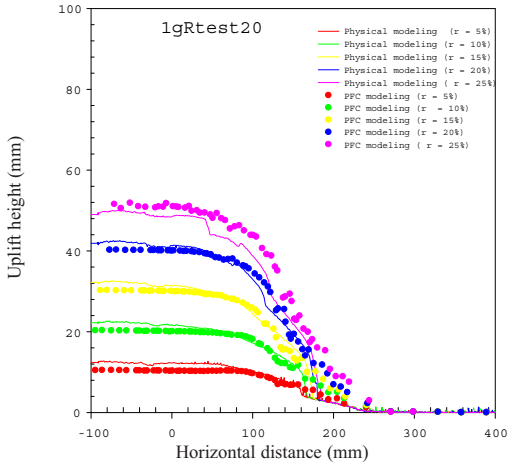

(a) at 1 g

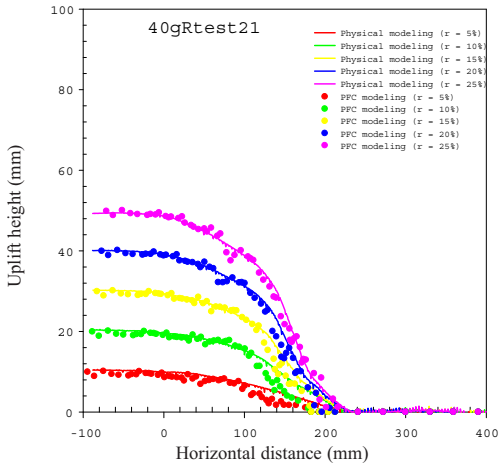

(b) at 40 g

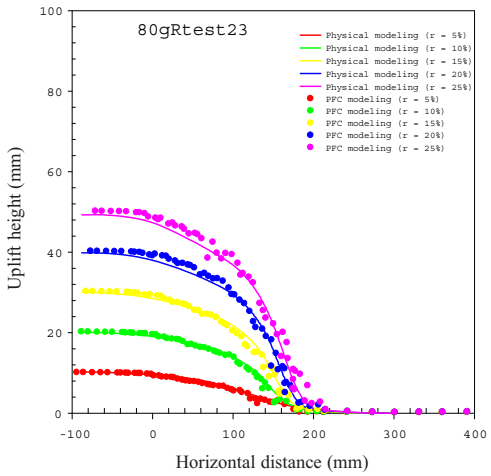

(c) numerical simulation at 80 g

Fig. 17 Comparison of surface deformation profiles measured from the physical model tests and those obtained from the PFC^{2D} simulation at the conditions of 1g, 40g, and 80g

(represented by dashed black lines) derived from the numerical simulation can be established using the same procedures adopted for the images of the centrifuge model. Figure 19 also shows the shear bands obtained from the physical model tests at various g levels (plotted with solid red lines)for comparison. The shear band numerically simulated at 80 g is the narrowest, whereas that simulated at 1 g is the widest, and that simulated at 40 lies in between.This figure shows the same trend as that obtained from the physical model tests. However, the numerical simulation exhibited a slightly wider shear band (approximately 20 wide, 1.6 m in prototype if simulated at 80 g) and an offset of 15 mm (1.2 m in prototype if simulated at 80 g) to the footwall than the physical model. This may be because the mean particle diameter of the disks used in the numerical simulation was 20 times larger than the mean grain size of the sand used in the physical model test. A larger mean particle size should produce a wider local shear band [10,18]. Therefore, the disks used in these numerical simulations should be as small as possible in future studies.

5. Conclusion

This study used a series of centrifuge model tests and the numerical simulation using PFC^{2D} to investigate the mechanism of reverse fault with a dip angle of 60° at the conditions of 1 g, 40 g, and 80 g. This study proposes a methodology of calibrating micromechanical material parameters used in the numerical simulation based on the measured surface settlements of the tested sand bed in the self-weight consolidation stage. The results of centrifuge modeling and numerical simulations lead to the following conclusions:

1. The surface deformation profiles have steeper surface slopes in the 1-g reverse faulting model test than the tests at higher g levels. The observed subsurface rupture pattern shows more faulting in the shallower depths in the 1-g test than in the higher g tests. The observed major faulting-induced distortion zone on the higher g model test also has a narrower shear band width. This may be because the small capillarity force developing among the sand particles increases the effective stresses in the soil mass, and a higher rate of dilation that occurs if the soil mass is tested at the 1g level or shallower depths.

2. The surface deformation profiles of the higher g physical modeling and numerical modeling show good agreement except for the 1g model test. Thus, the PFC^{2D} associated with the proposed calibration methodology on the material parameters used in PFC^{2D} can accurately predict the surface deformation profiles at various vertical throws in reverse faulting events.

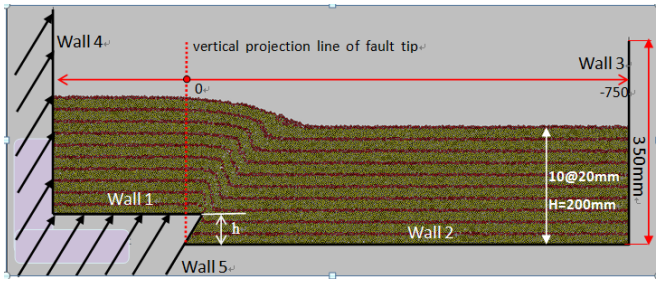

Fig. 18 Displacement pattern of the marked layers in the numerical specimen simulated at 80 g

3. The narrow shear bands were obtained from both the higher g physical model tests and the higher g numerical simulation. However, the numerical simulation gave a slightly wider shear band and an offset of 15 mm to the footwall compared with the results of physical modeling.

4. The test results of centrifuge experiments validated the numerical results, emphasizing the surface deformation profiles and the subsurface rupture patterns.

Acknowledgments: This study was sponsored by the Central Geological Survey (CGS), Ministry of Economic Affairs, Taiwan (100-5226904000-05-01& 101-5226904000-03-01). The authors would like to express their gratitude for the financial and technical supports, which have made this study and future researches possible.

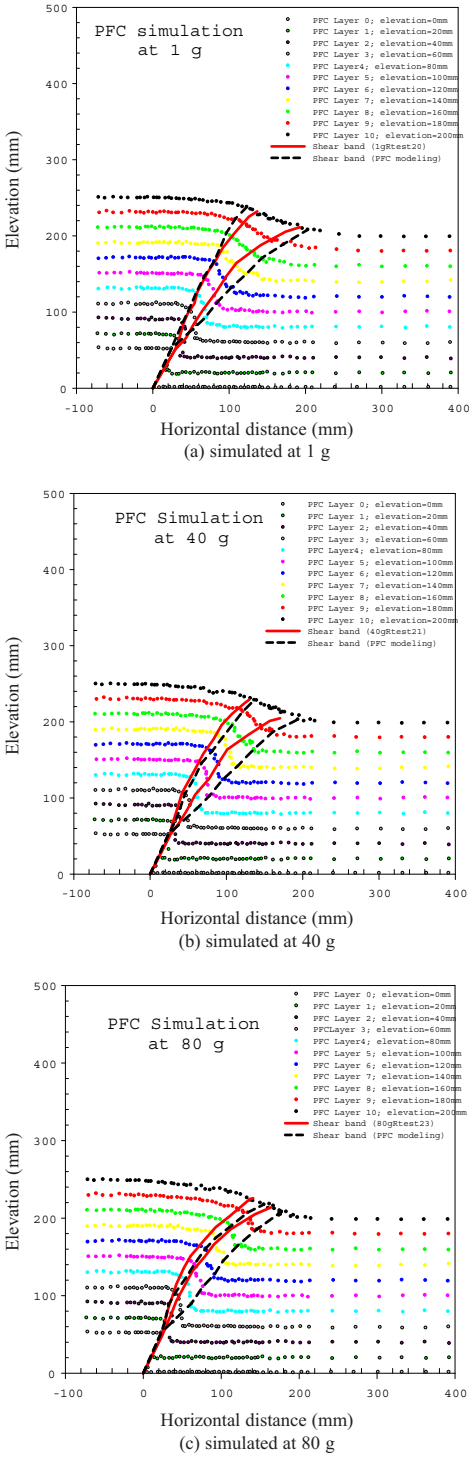

Fig. 19 Displacement patterns of the marked layers and the comparison of the major faulting-induced distortion zone in the numerical specimen and physical modeling simulated at (a) 1 g; (b) 40 g; (c) 80 g

References

[1] Ulusay R, AydanO¨, Hamada M. The behaviour of structures built on active fault zones: examples from the recent earthquakes in Turkey. Seismic fault-induced failures.2001; p.1–26.

[2] Dong J.J., Wang C.D., Lee C.T., Liao J.J., Pan Y.W., The influence of surface ruptures on building damage in the 1999 Chi-Chi earthquake: a case study in Fengyuan City,Engineering Geology, 2004;71(1–2),157–79.

[3] Chen C.C., Huang C.T., Cherng R.H., Jeng V. Preliminary investigation of damage to near fault buildings of the 1999 Chi-Chi earthquake,Earthquake Engineering and Engineering Seismology, 2000;2(1),79–92.

[4] Lin M.L., Chung C.F., Jeng F.S. Deformation of overburden soil induced by thrust fault slip,Engineering Geology, 2006;88(1–2),70–89.

[5] Bransby M.F., Davies M.C.R., EINahas A. Centrifuge modelling of normal fault–foundation interaction,Bulletin of Earthquake Engineering, 2008;6(4),585–605.

[6] Moosavi S. M., Jafari M. K., Kamalian M.,Shafiee A.Experimental Investigation of Reverse Fault Rupture–Rigid Shallow Foundation Interaction,International Journal of Civil Engineering, 2010; 8(2),85-98.

[7] Anastasopoulos I., Gazetas G. Foundation–structure systems over a rupturing normal fault: part II. Analysis of the Kocaeli case histories,Bulletin of Earthquake Engineering, 2007;5(3),277–301.

[8] Loukidis D., Bouckovalas G., Papadimitriou A. Analysis of fault rupture propagation through uniform soil cover, Soil Dynamics and Earthquake Engineering, 2009;(29),1389-1404.

[9] Anastasopoulos I., Gazetas G., Bransby, M.F., Davies, M.C.R., EI Nahas, A. Fault rupture propagation through sand: Finite-Element analysis and validation through experiments, Journal of Geotechnical and Geoenviromental Engineering, 2007; 133(8),943-958.

[10] White, R.J., Stone,K.J.L., Jewell, R.J. Effect of particle size on localization development in model test on sand. Centrifuge 94, Leung, Lee, and Tan eds. Malkema, Rotterdam, The Netherlands, 1994, pp.817-822.

[11] Nakai, T., Muir Wood, D., Stone, K.J.L. Numerical calculations of soil response over a displacing basement, Soils and Foundations, 1995; 35(2),25-35.

[12] Cundall P.A., Strack O.D.L. A discrete numerical model for granular assemblies, Geotechnique,1979;29(1),47-65.

[13] Lee C.J., Wang C.R., Wei Y.C., Hung W.Y. Evolution of the shear wave velocity during shaking modeled in centrifuge shaking table tests, Bulletin of Earthquake Engineering, 2012;10(2),401-420.

[14] Bolton MD. The strength and dilatancy of sands, Geotechnique, 1986; 36(1),65-78

[15] Ting J.M., Corkum B.T., Kkauffman C.R., Creco C. Discrete numerical model for soil mechanics, Journal of Geotechnical Engineering, ASCE,1990; 115(30), 379-398.

[16] Powrie W., Ni Q., Harkness R. Numerical modeling of plane strain tests on sand using a particulate approach, Geotechnique, 2005; 55(4),297-306.

[17] Yimsiri S., Soga K. Micromechanics-based stress-strain behaviour of soils at small strains, Geotechnique, 2000;50(1),559-571

[18] Stone, K, Wood, DM. Effects of dilatancy and particle size observed in model tests on sands,Soils and Foundations, 1992; 32(4),43-57.